Particle & Particle Systems Characterization
www.particle-journal.com

TEMAS: A Flexible Non-AI Algorithm for Metrology of Single-Core and Core-Shell Nanoparticles from TEM Images

*Jorge J. Sáenz Noval, Rubén Gómez-Merchán, Juan A. Leñero-Bardallo, and Lionel C. Gontard**

An essential application of electron microscopy is to provide feedback to tune the fabrication of nanoparticles (NPs). Real samples tend to follow a size distribution commonly linked to the synthesis process used and in turn to their functional properties. This study presents an algorithm for measuring particle size distributions in electron microscopy images. State-of-the-art methods based on Artificial Intelligence (e.g., Deep Learning) require extensive datasets of labeled images similar to those expected to be analyzed, and extensive supervised re-training is often required for cross-domain application. In contrast, the non-AI algorithm described in this study is accurate and can be quickly set up for measuring new experimental images in different domains. The accuracy of the method is validated quantitatively and comparing graphical and descriptive statistics. Different size distributions are measured on images of platinum and gold nanocatalysts supported on carbon black, amorphous carbon, and titanium dioxide crystals. Also, images of platinum-iron core-shell NPs supported on thin amorphous carbon film are successfully analyzed. The limitation of evaluating different algorithms for NPs metrology is the lack of standards that different researchers can use as ground truth. In order to overcome this limitation, the images and the ground truth measurements presented here are shared as an open dataset.

1. Introduction

Nanoparticles (NPs) are used in a wide range of applications, with many of their physical and chemical properties being size-dependent.[1] For instance, the catalytic treatment (e.g., high operating temperature) of supported metals can change the metal surface area due to processes such as sintering, resulting in a decrease in exposed surface area and hence in catalytic activity. Therefore, particle size distributions (PSDs) of NPs are routinely measured in industrial environments, with the requirement that they should be statistically reproducible, meaningful, and accurate.

The two complementary techniques typically used for measuring PSDs are transmission electron microscopy (TEM) and X-ray diffraction (XRD). The deconvolution of XRD patterns is challenging. The mean crystal size is calculated over millions of scattering elements that can be misleading if the particles have multiple crystalline domains, e.g., twinned particles, core-shell particles, etc.[2,3] TEM, on the other hand, produces images containing hundreds or thousands of particles whose size distribution is measured with digital image processing techniques that are combined with algorithms for shape analysis and classification. Recently, it has been demonstrated that the application of genetic algorithms or supervised/unsupervised Artificial Intelligence (AI) methods for shape classification increases the quality and amount of information that can be extracted from TEM images.[4–7] The starting point of any image-based method is separating the particles from the background, a procedure called image segmentation. The most basic approach is an intensity-based segmentation that uses a global threshold value for classifying image pixels into two classes, particle or background.[8,9] In most cases, that simple approach fails due to particle overlapping or local variations of the diffraction conditions and the composition across the field-of-view. Better results are thus obtained by optimising the threshold according to the local intensities in the image.[10–12] The fact that in many practical cases NPs can be approximated to circles has been exploited to detect the NPs either using a Laplacian of Gaussian filter, that is a blob-detector that responds to circular image structures, or by fitting simple intensity

J. J. S. Noval, L. C. Gontard
Department of Condensed Matter Physics
Applied Magnetism and Optics Research Group
University of Cádiz
11510 Puerto Real, Spain
E-mail: lionel.cervera@uca.es
J. J. S. Noval, L. C. Gontard
IMEYMAT
University of Cádiz
11510 Puerto Real, Spain
R. Gómez-Merchán, J. A. Leñero-Bardallo
Institute of Microelectronics of Seville (IMSE-CNM)
CSIC-Universidad de Sevilla
41092 Sevilla, Spain
The ORCID identification number(s) for the author(s) of this article can be found under https://doi.org/10.1002/ppsc.202200170.

DOI: 10.1002/ppsc.202200170

models of the projected shapes to the TEM image.[13,14] Also the identification of NPs edges using the circular Hough transform is a powerful method that can perform well with images with low-contrast and it is particularly useful for separating overlapping particles.[15,16] The main limitation is that these methods are useful for detecting explicitly predefined geometries. AI approaches are the state-of-the-art in image analysis tasks, and supervised Deep Learning for image segmentation has demonstrated the potential for NP metrology in electron microscopy.[4,5,7,17–19] Nevertheless, the generalization of AI models to different domains (different types of samples and imaging conditions) in electron microscopy has not been demonstrated yet. Setting up the software environment for implementing Deep Learning is still overwhelming, data collection and preparation is not an obvious task, and training the AI model requires large amounts of annotated data, thus rendering it often inaccessible to most microscopy users.

Template matching is a conventional yet powerful approach that can detect patterns in images but it has been largely unexplored for its application for the metrology of NPs.[20–22] This work presents TEMAS, TEmplate Matching and Adaptive Segmentation, a non-AI algorithm for measuring PSDs that is simultaneously accurate and flexible (see **Figure 1**). The method is validated using statistical analysis of the PSDs measured on different samples acquired with different imaging conditions which are then compared to a ground truth.

2. Nanoparticle Metrology Workflow

2.1. Algorithm Description

Figure 2 shows an example of a bright-field TEM image of Pt catalyst NPs supported on carbon black (see sample description in the Experimental Section and **Table 1**). The image is in gray scale and contains hundreds of similar NPs with sizes that are a fraction of the field-of-view size, and with an average pixel intensity that changes strongly from particle to particle. The image represents the type of sample that is routinely analyzed in the industry of nanocatalysts and from which the detection, measurement and classification of the particles are of interest.[23]

TEMAS is based on performing segmentation of Regions-of-Interest (ROIs) of the image containing approximately one NP that are detected using template matching. The algorithm consists of the following steps (see also flowchart in Figure 1):

1) Generating a collection of templates,
2) Template matching for detecting candidates ROIs containing single NPs,
3) Keeping one representative ROI for each NP using the "Non-maximum Suppression" (NMS) algorithm,
4) Segmenting each ROI using Otsu's thresholding,
5) Filtering the binary ROIs, and
6) Blob analysis of the binary ROIs using the Area-equivalent diameter.

The steps are detailed in the following sections and in the Experimental Section.

2.1.1. NPs Detection Using Multi-Template Matching

TEMAS uses template matching to localize individual NPs across the image. First, the target image is scanned by one template, which is an image containing one NP. The template can be cropped from the target image or from another image similar to the one to be analyzed. Second, a similarity index between the template and the local patch of the target image is calculated at each position (see Experimental Section for implementation details). Finally, the positions with the most significant similarities are identified as potential ROIs containing one NP. The similarity metric used in TEMAS is the normalized cross-correlation function that outputs a value between 0 and 1. The closer to 1, the more likely is the patch of the image contains an NP. The selection criteria used in this work to select or reject an ROI is that the patch has a similarity ≥ 0.5. The number of particles detected (and also false positives) can be increased by decreasing the similarity threshold used during the template matching step. On the contrary, the number of undetected particles (or false negatives) increases when the similarity index is raised. We found in our experiments that using a threshold of 0.5 most of the particles present in the image were detected while false positives were kept to a minimum (when combined with the algorithm NMS explained in the following section).

In general, template matching is more robust if it is rotation and scale invariant. Because NPs have frequently circular symmetry, we did not considered rotating the templates. Regarding to scale, we increased the NP detection capacity in TEMAS using template matching successively with a collection of templates (or multi-template matching) that can better represent the types and sizes of NPs present in the image (see Figure 1). Therefore, for the application of TEMAS, the user must select several templates containing one NP. The NPs tend to be very similar

Table 1. Description of the samples and imaging parameters.

	Sample 1	Sample 2	Sample 3	Sample 4	Sample 5
NPs composition	*Pt*, N_2 @ 900 °C	*Pt*	*Pt*	core-shell $PtFe@Fe_xO_y$	*Au*
Sample support	Carbon black	Carbon black	Carbon black	Amorphous *C* film	Crystalline TiO_2
Microscope	Tecnai F20	Tecnai F20	Philips CM200 LaB_6	Tecnai G2 F30	Tecnai T20
Sensor type	CCD	CCD	Digitized film	CMOS	CCD
Image size (pixels)	2048 × 2048	2048 × 2048	1956 × 1257	958 × 958	2048 × 2048
File Format	bmp	jpg	tif	png	png

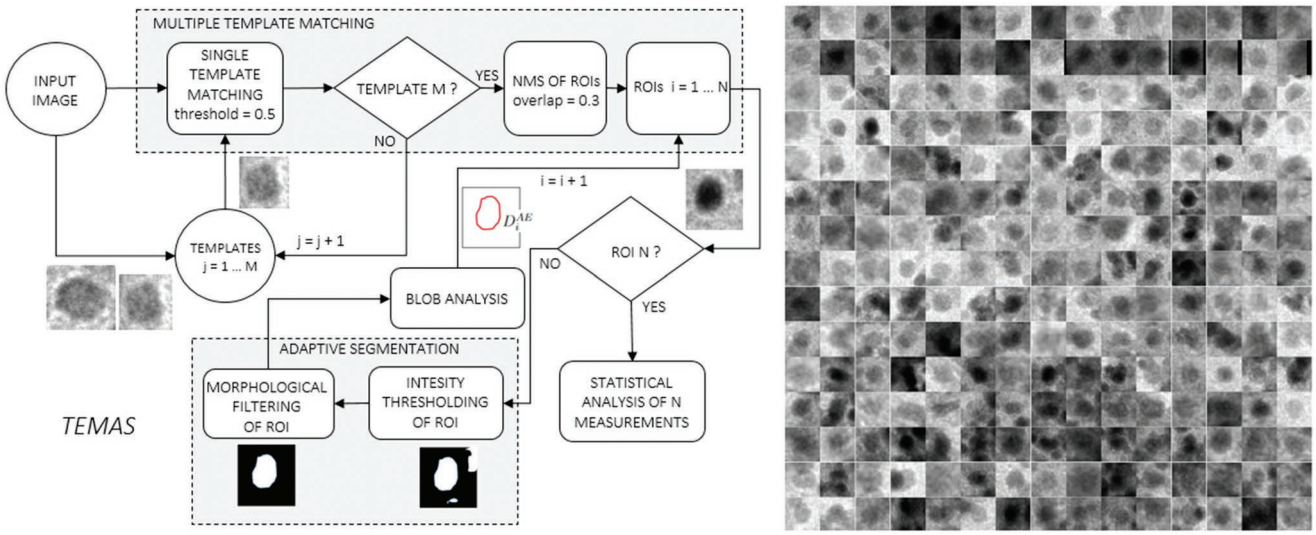

Figure 1. In the left, is the algorithm's flowchart for measuring PSDs called TEMAS. In this concrete example, adaptive segmentation is done using intensity thresholding. Right, a selection of 225 ROIs containing approximately one NPs each. The ROIs were detected using multiple template matching.

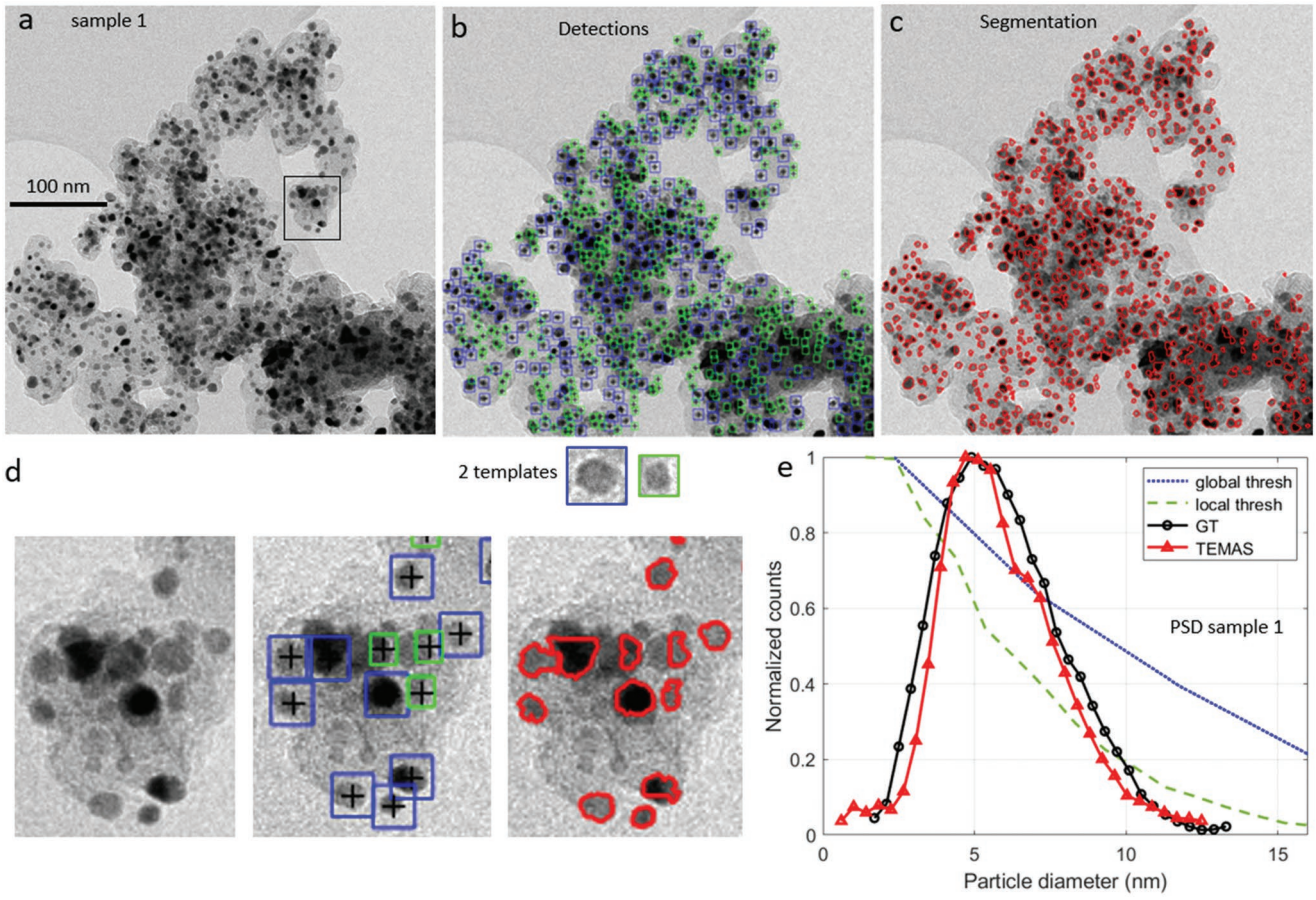

Figure 2. a) Bright-field TEM image of Pt catalysts supported on carbon black (sample 1 described in Table 1). b) Image annotated with ROIs containing NPs. The ROIs were localized using template matching with the two templates shown below the image. c) Contours of NPs segmented in each ROI. d) Detail of the results of the region marked inside the black square in a). e) Histograms of the PSD measured using local thresholding, global thresholding, TEMAS and manual segmentation (ground truth or GT).

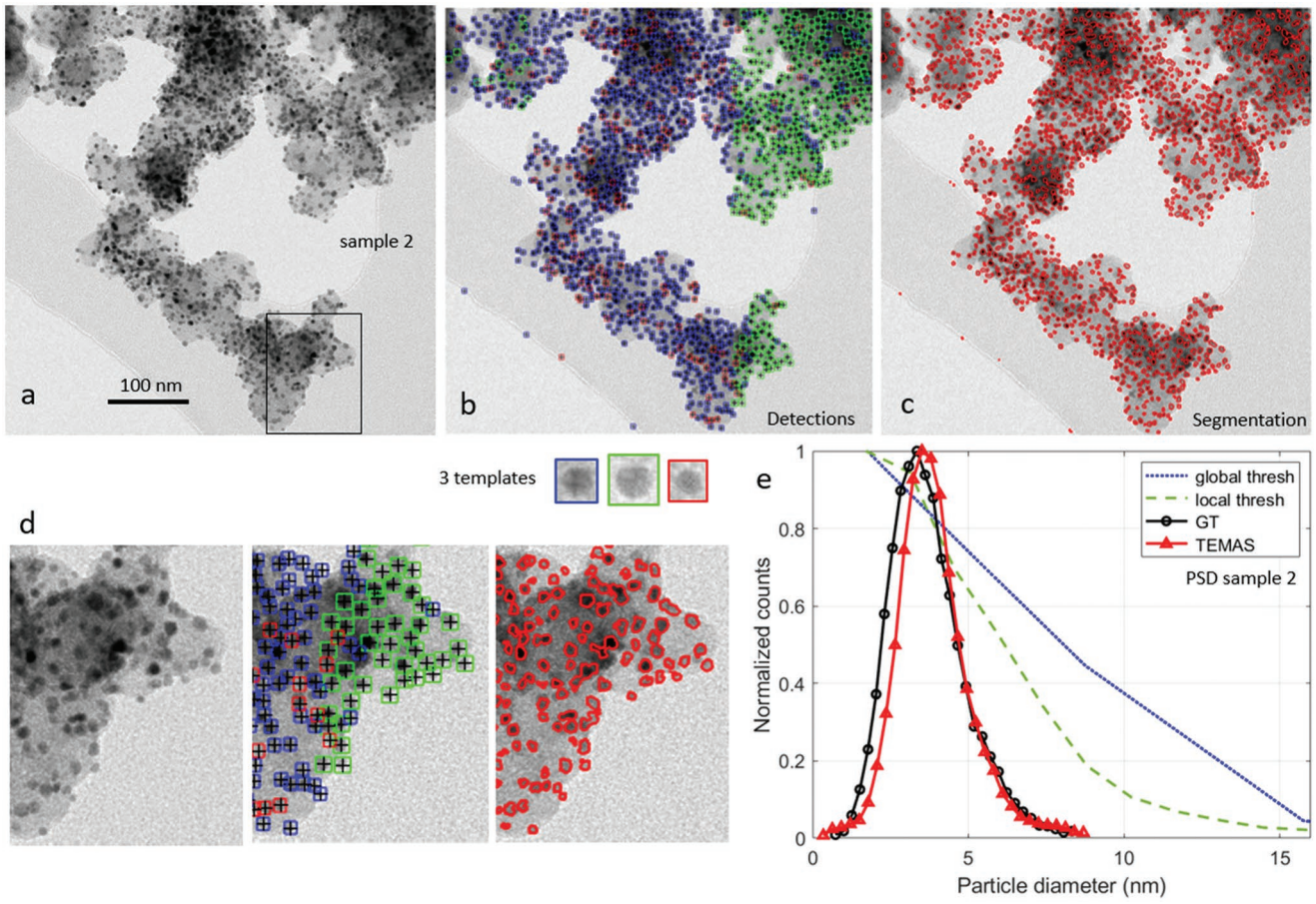

Figure 3. PSD of a sample of Pt nanocatalysts (sample 2) measured using *TEMAS* with three templates.

except for intensity and size variations, hence 2–3 templates are enough to represent the variability of particles. For example, Figure 2c shows the application TEMAS using two templates of two NPs of different sizes cropped from the TEM image.

2.1.2. ROIs Selection Using NMS

Template matching performs a window scanning across the image to be analyzed with a stride that is smaller than the ROI dimensions. Windows close to each other can result in several ROIs pointing to the same NP. For this reason, it is necessary to devise a method to sift through the proposed ROIs and filter them to keep only one ROI representative of one NP. The task consists of selecting an ROI among many overlapping ones and in TEMAS this is done using NMS,[24,25] which is the most straightforward and efficient algorithm for this task. The selection criteria used in this work for selecting or rejecting an ROI with NMS is that the patches have an overlap ≤ 0.3 And the output of this step is a selection of N ROIs which have less than 30% of mutual overlapping.

2.1.3. Adaptive Segmentation

After detecting N patches (or ROIs) containing approximately one NP each, it is necessary to segment them to label its pixels. In TEMAS, Otsu's method is used to determine the optimal thresholds for separating the NP from the image background.[8] For the samples containing single-core NPs (see examples in the **Figures 2–4**) only one threshold was calculated using Otsu's method, the resulting binary ROIs contained blobs formed by groups of pixels classified into two classes (core, support). For samples made of core-shell NPs (see **Figure 5**), we segmented the image using a multi-Otsu approach to find two optimal thresholds in each of the N ROIs. After segmentation, the ROIs contain blobs of three classes (core, shell, support).

2.1.4. Morphological Filtering and Blob Analysis

The ROIs are filtered using an opening operator (erosion followed by dilation) to smooth the boundaries of the blobs by removing small protrusions, to break narrow isthmuses thus separating the touching particles, and to reduce noise by removing regions smaller than the size of a chosen structuring element. In the examples shown in this work, the opening operator was applied with a circular structuring element with a radius of 3 pixels. The final step in TEMAS consists in doing a blob analysis of each ROI. To reduce the potential error of measuring portions of nearby NPs cropped by the ROI only the largest blob is kept in each ROI.

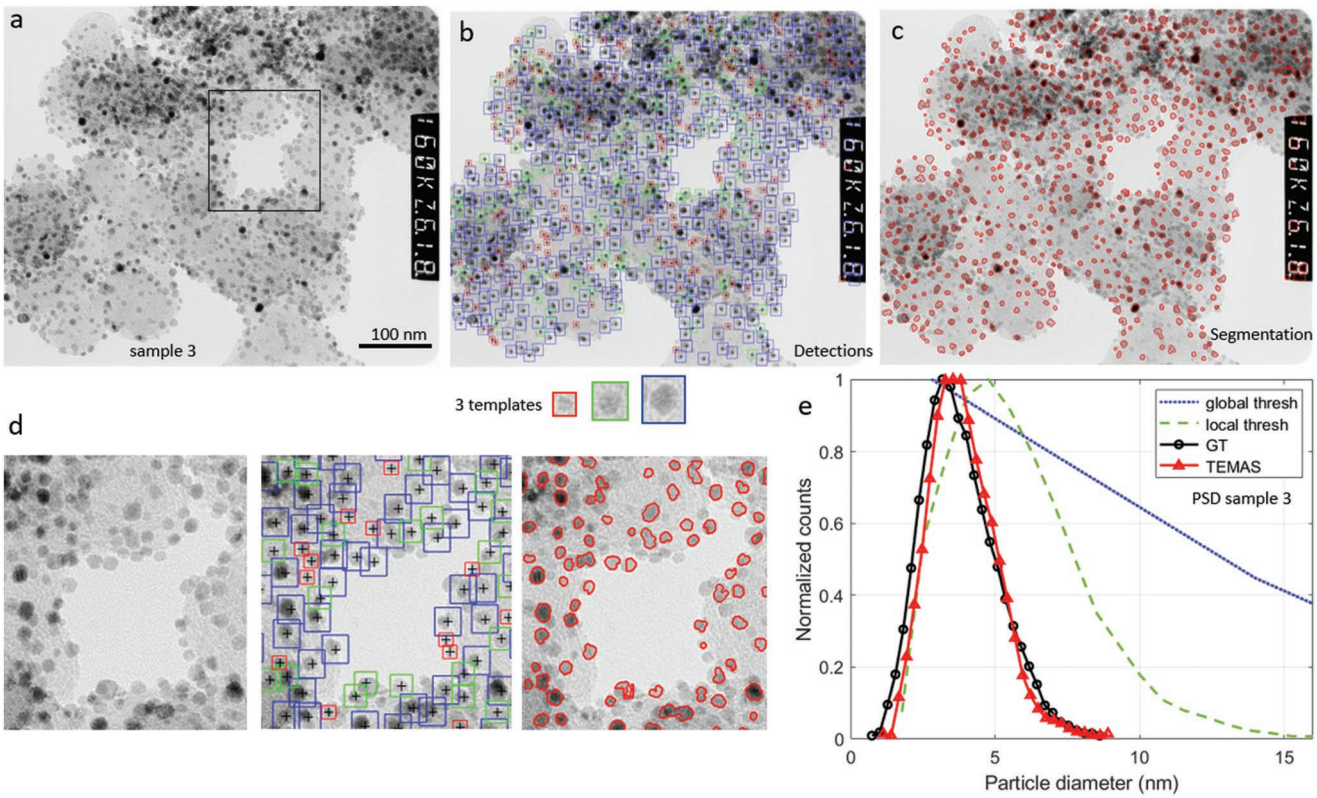

Figure 4. PSD of a sample of Pt nanocatalysts (sample 3) measured using *TEMAS* with three templates.

2.2. Validation

2.2.1. Statistical Analysis

TEMAS was applied to five TEM images of single-core and core-shell NPs supported on different materials, and acquired with different imaging conditions (see the description in Table 1). The results are displayed in the **Figures 2–8** and compiled in **Tables 2** and **3**.

Each figure displays: a) the original image, b) the original image with the overlays of boxes corresponding with ROIs selected, c) the original image with the overlay of the contours of the segmented NPs, d) detail of a), b), and c) and the templates used, and e) a graph with the plots of four histograms of the PSDs as calculated using different methods: TEMAS, ground truth measured using manual segmentation ("GT"), global thresholding ("global thresh") and adaptive thresholding ("local thresh"), as described in the Experimental Section.

The PSDs were characterized using the following statistical parameters:[26] the number of counts, *N*, the minimum and maximum diameter, $\min(D_i)$ and $\mathrm{Max}(D_i)$, the arithmetic *mean*, $\overline{D}^{AE}$, the *Median*, and the standard deviation, *std*. Descriptive statistic can be misleading in some cases. For example, the standard deviation is very sensitive to the presence of a small number of outliers. Hence, we also evaluated the similarity of the shapes of the distributions with respect to the ground truth measured manually by comparing the graphs qualitatively, and computing numerically the *p*-value and *D** of the "Two Sample Kolmogorov–Smirnov Test".

2.2.2. Time Performance

Regarding computation speed, template matching tends to be slow because it requires a search over the whole input space for all (or part of) transformation space.[27] We found that in our experiments the total processing time (see Figure 8) of each image using TEMAS is proportional to *NM* being *N* the number of particles detected in the image and *M* the number of templates applied. Using our computational approach, a single particle measurement takes an average of 75 µs.

3. Discussion

The results demonstrate a remarkable correspondence between the PSDs obtained using TEMAS and the GTs. In contrast, the results obtained using alternative segmentation methods like Local and Global thresholding display significant errors.

The mean Area-equivalent diameter error using TEMAS for the five samples ranges between 0% for sample 1 and 7.7% for the shells of sample 4, and the mean error of the five samples is 3.8%. TEMAS is accurate also for classifying the mixture of single-core and core-shell NPs of sample 4. A 14% of the NPs do not have shells according to the ground truth (and 11% with TEMAS). The mean size of samples 1–3 is larger than the Median, indicating that the Pt NPs follow a lognormal distribution skewed right as expected for this type of sample.[2] A *p*-value closer to 1, which corresponds to a small *D**, indicates

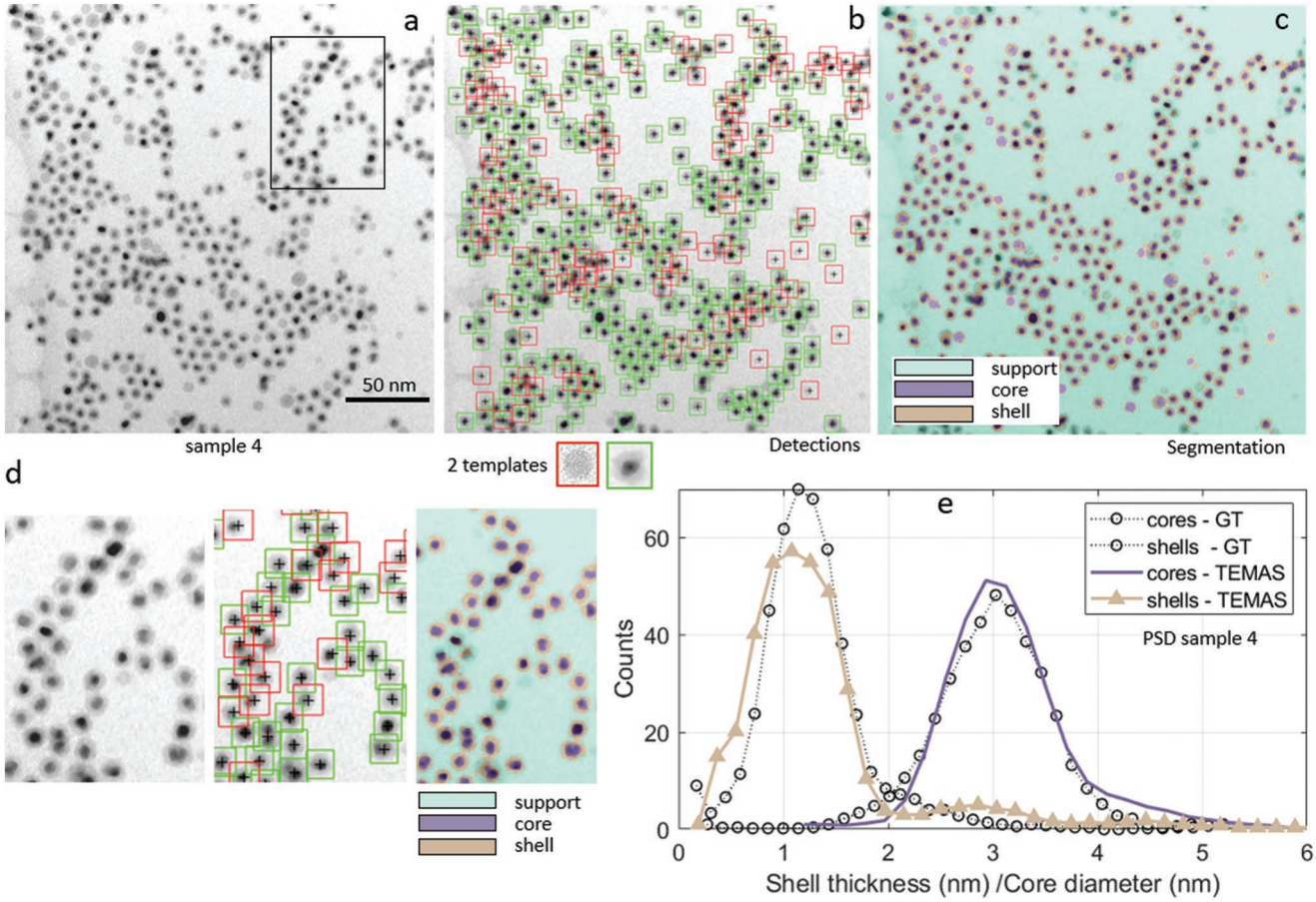

Figure 5. a) TEM image of a sample of $PtFe@Fe_xO_y$ core-shell nanoparticles (sample 4) deposited directly onto the carbon film of a TEM grid following hexane evaporation. b) Image annotated with ROIs containing NPs. The ROIs were localized using template matching with the two templates shown below the image. c) Image colored with the three classes of pixels: background, cores and shells. d) Detail of the results of the region inside the black square in (a). e) Histograms of the size distributions of the cores and the shells measured using local thresholding, global thresholding, *TEMAS* and manual segmentation (ground truth or GT).

a good fit of two distributions.[10] According to the *p*-value and *D** values obtained, TEMAS provide size distributions that are much closer to the GT distributions (the "real" ones) than when using Global or Local thresholding. The contribution of false negatives and false positives particles is smoothed by the big number of particles analyzed. TEMAS' accuracy can be fine-tuned for particular problems by changing the cross-correlation threshold, and the overlapping value.

The main limitation for increasing the generalization capacities of AI models is the lack of annotated data that conveniently represent the variability of images be found in a specific domain (i.e., specific imaging modes and different types of samples). In this context, methodologies for synthetic image generation using image simulations[28] or photo-realistic rendering[29] are being proposed. However, these methods require explicitly creating the datasets for each different type of sample and technique. TEMAS can be used also for processing quickly a collection of TEM images to build an extensive database with thousands of 2D ROIs and their labels which can be used for training Deep Learning models.

The accuracy obtained with TEMAS may be similar to that of Deep Learning models based on Convolutional Neural Networks, CNNs. Recently, it has been shown that a CNN with only one convolutional layer can be enough to learn meaningful features of NPs with comparable accuracy to the output of a deep CNN.[30] In a very simple description, CNNs contain sequential layers of image filters (equivalent to templates), which are then computed across the image using convolutions (equivalent to cross-correlation except for a sign and how we access the coordinates of the image). In this respect, TEMAS can be see as a shallow CNN with a convolutional layer with a few filters (equal to the number of templates used), in which instead of training the filters using supervised learning, a human select 2 or 3 templates to be used by the algorithm. This hybrid human-automated approach adds flexibility to TEMAS being an advantage compared to CNN models that need to be retrained for new domains.

TEMAS is very flexible as templates can be easily found for specific application domain.The flexibility of TEMAS has been demonstrated for different electron microscopy imaging modes and samples: single-core gold NPs supported on big 3D-supports as

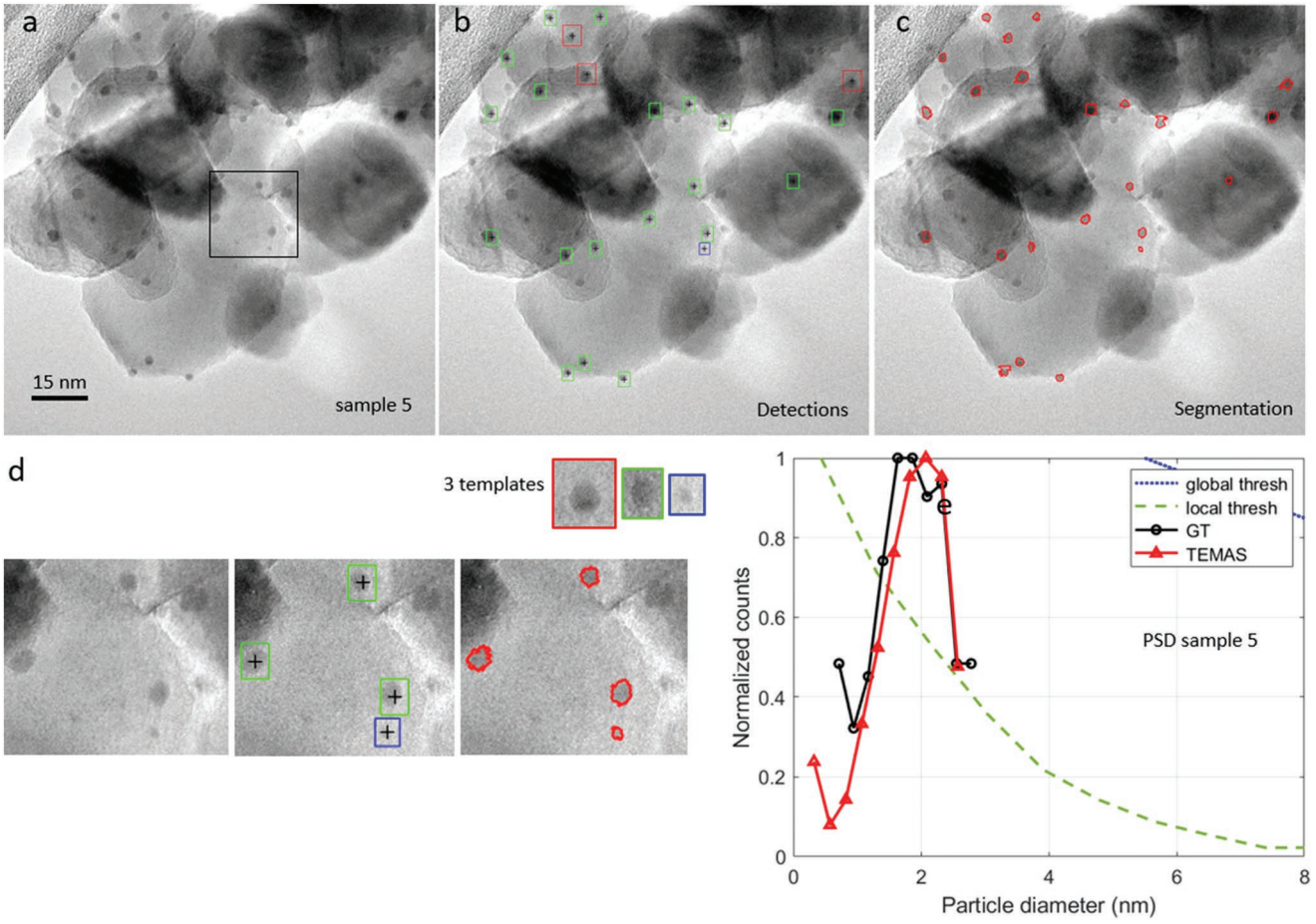

Figure 6. Bright-field TEM image of Au NPs (sample 5) supported on crystals of TiO_2.

in the Figures 2–4 and 6, core-shell NPs supported on thin films in Bright-field TEM mode as in the Figure 5 or for an aberration corrected high-resolution scanning TEM (STEM) image of NPs acquired in high-angle annular dark-field mode as in the Figure 7.

TEMAS deals with the common problem of NP overlapping in two ways. Firstly, the NMS algorithm keeps only one NP of a group of overlapping ROIs (or NPs) and rejects the others. And secondly, the multi-template matching step outputs ROIs

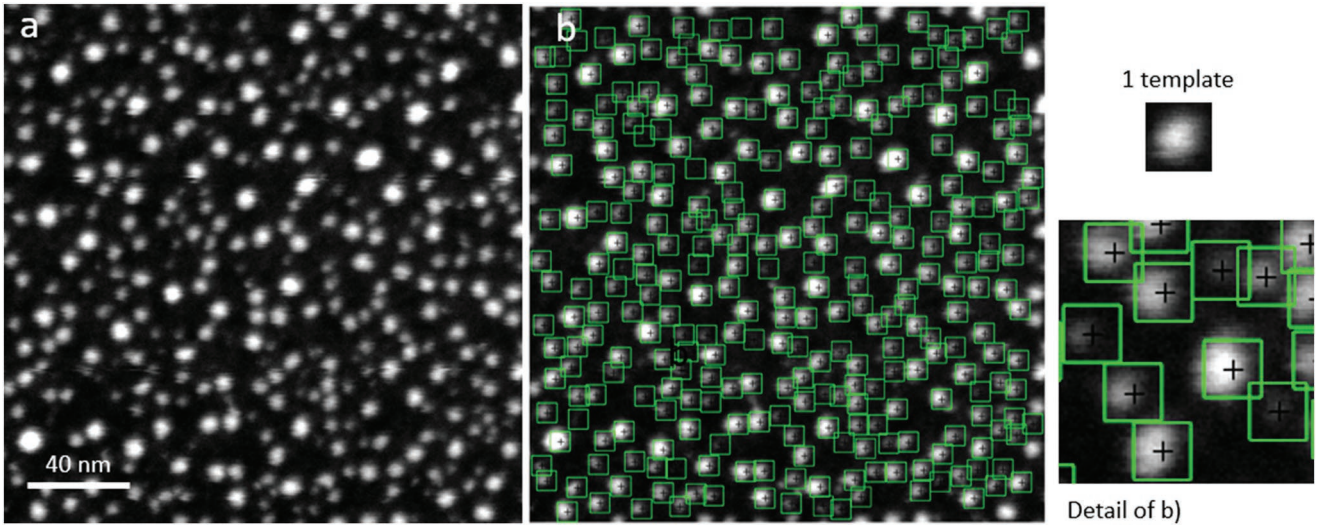

Figure 7. Dark-field scanning TEM (STEM) image of hybrid Au NPs supported on an amorphous carbon film.

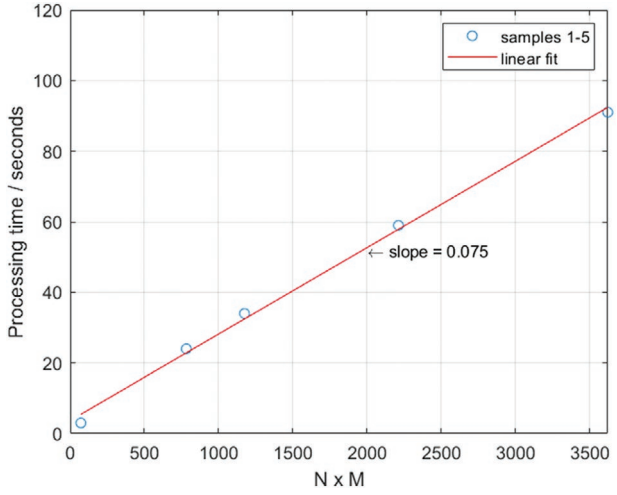

Figure 8. The processing time of TEMAS is linear with *NM* being *N* the number of particles detected and *M* the number of templates used.

containing approximately one NPs, by cropping neighbouring touching particles. Improvements to TEMAS for dealing with overlapping particles and segmentation accuracy can also be made by applying better methods of segmenting the ROIs, for example, applying the circular Hough transform or Deep Learning instance-based segmentation instead of using simple intensity-thresholding methods.

4. Conclusion

It has been described an algorithm called TEMAS that can be used for accurately measuring PSDs using a combination of multiple templates matching and adaptive intensity thresholding. It has been validated graphically and quantitatively on complex TEM images of single-core and core-shell NPs. The results demonstrate a remarkable correspondence with ground truth data. TEMAS is not suitable for real-time applications but the algorithm is very flexible, and the only requirement is to have access to a few templates extracted from images of the application domain of interest. NPs have frequently circular symmetry and similar sizes, nevertheless, the generalization of TEMAS can be improved for more complex shapes by using scale and rotation invariant template matching. Finally, we also propose that TEMAS can be of interest for generating large datasets of annotated NPs required for training Deep Learning models with application to NP metrology.

5. Experimental Section

Samples Description: Samples 2 and 3 were carbon-supported (Vulcan XC-72R) platinum particles (19.1 wt.%) provided by the Johnson Matthey Technology Centre. Sample 1 was similar to sample 2 and 3 but that after synthesis was further reduced in a rich N_2 atmosphere at 900 °C. For studying samples in the electron microscope, dry powders were directly dispersed onto holey carbon TEM copper grids. These samples were used as electrocatalysts in Proton Membrane fuel cells which require high loadings of platinum, and must be able to provide high electrical conductivity, good reactant gas access, adequate water handling, and good corrosion resistance. Electrocatalysts with high dispersions are typically supported on mesoporous high-surface-area carbon blacks $\left(>75\frac{m^2}{g}\right)$. Carbon black is a low-grade form of graphite, composed of crystallites and lacks 3D order. Sample 4 consisted of $PtFe@Fe_xO_y$ core-shell NPs deposited directly onto the carbon film of a TEM grid following hexane evaporation.[31] Sample 5 composed of powder catalysts of Au NPs supported on crystalline oxides had been prepared by carefully developed methods involving gold precipitation from solution.[32] Figure 7 is an aberration-corrected HAADF STEM image of 5 nm *Au* NPs capped with dodecanethiols (Au-SR) supported on a thin amorphous carbon film.[33]

Local and Global Thresholding: For local and global thresholding, the greyscale images were converted into a binary image using the *Otsu*'s method and filtered with an opening operator with a circular kernel of 5 pixels. For local thresholding, different parts of an image were selected naively in a regular grid.[11] Global and Local thresholding methods were applied to the images of single-core NPs shown in Figures 1–6. The curves of the corresponding PSDs measured using both methods are labeled in the figures as "local thresh" and "global thresh."

Computer Implementation: The algorithm was implemented with the software MATLAB 2021a and in a PC Intel Core i5-9300H CPU @ 2.40 GHz and with 32 GB of RAM.

Table 2. Statistical measurements of the PSDs of platinum NPs.

	Sample 1	Sample 2	Sample 3
Measures	GT/TEMAS/Local/Global	GT/TEMAS/Local/Global	GT/TEMAS/Local/Global
N	567/**587**/849/338	1130/1207/2508/**1105**	1206/737/1036/**1312**
$\overline{D}^{AE}$ [nm] (error %)	5.9/**5.9** (0%)/5.0/7.0	3.7/**3.9** (5.4%)/4.8/5.8	3.8/**3.9** (2.6%)/5.6/8.8
Median [nm] (error %)	5.6/**5.6** (0%)/4.0/4.7	3.7/3.5 (5.4%)/**3.8**/**3.8**	3.8/**3.6** (5.2%)/5.2/6.0
std [nm] (error %)	2.0/**2.0** (0%)/3.5/10.2	1.2/ **1.1** (8.3%)/4.0/10.0	1.3/**1.1** (15.1%)/2.4/13.4
$\min(D_i^{AE})$ [nm]	1.7/0.5/1.0/**1.4**	0.7/**0.4**/1.0/1.3	0.7/**1.1**/1.6/2.2
$\mathrm{Max}(D_i^{AE})$ [nm]	13.0/**13.0**/20.0/140.0	8.5/**8.8**/44.0/102.0	8.7/**9.0**/24.0/168.0
D^*	–/**0.0635**/0.3647/0.266	–/ **0.1394**/0.1777/0.1723	–/**0.1035**/0.3696/0.5102
p-value	–/**0.1884**/$<10^{-5}$/10^{-13}	–/**<10**$^{-9}$/$<10^{-21}$/$<10^{-14}$	–/**<10**$^{-4}$/$<10^{-66}$/$<10^{-143}$
Total time [s]	≈3600/34/–/–	≈6000/91/–/–	≈6000/59/–/–
Time per ROI [s]	–/61×10^{-6}/–/–	–/75×10^{-6}/–/–	–/81×10^{-6}/–/–
Number of templates	2	3	3

Table 3. Statistical measurements of the PSDs of core-shells and gold NPs.

	Sample 4			Sample 5
	Cores	Shells	Single particle	
Measures	GT/TEMAS	GT/TEMAS	GT/TEMAS	GT/TEMAS/Local/Global
N (percentage of total %)	403/347	469/391	66 (14%)/44(11%)	43/**24**/392/594
$\overline{D}^{AE}$ [nm] (error %)	3.0/3.1 (3.3%)	1.3/1.4 (7.7%)		1.9/**1.9** (0%)/1.9/1.2
Median [nm] (error %)	3.1/3.0 (3.3%)	1.2/1.2 (0%)		1.9/**1.9** (0%)/0.68/0.33
std [nm] (error %)	0.5/0.6 (20%)	0.5/0.8 (60%)		0.5/**0.5** (0%)/1.6/5.0
$\min(D_i^{AE})$ [nm]	0.2/1.2	0.1/0.2		0.7/0.3/0.2/**0.5**
$\mathrm{Max}(D_i^{AE})$ [nm]	5.2/7.8	4.9/6.3		2.8/**2.7**/8.7/1100
D^*	–/0.01910	–/0.12740		–/**0.1541**/0.631/0.9242
p-value	–/1.0000	–/0.0170		–/**0.8259**/$<10^{-13}$/$<10^{-30}$
Total time [s]	≈4700/24	≈4700/24		≈360/3.0
Time per ROI [s]	$-/61\times10^{-6}$	$-/61\times10^{-6}$		$-/125\times10^{-6}$/ –/–
Number of templates	2			3

For template matching, the normalized cross-correlation was calculated across the images using the function *normxcorr2* which provides a similarity index between [0, 1] for each position of the template positioned at the image coordinates (u, v), and it is defined like

$$\gamma(u,v)=\frac{\sum_{x,y}[f(x,y)-\overline{f}_{u,v}][t(x-u,y-v)-\bar{t}]}{\sqrt{\sum_{x,y}[f(x,y)-\overline{f}_{u,v}]^2\sum_{x,y}[t(x-u,y-v)-\bar{t}]^2}} \quad (1)$$

where f is the image, t is the template, $\bar{t}$ is the mean intensity of the template, and $f_{u,v}$ is the mean intensity of the image under the template.

Regarding the implementation of the algorithm NMS an optimized code can be found in Ref. [34]. Intensity thresholding was applied using the function *multithresh*. Alternatively, similar functions can be found for the language Python. Template matching is available within the OpenCV library as *cv.matchTemplate* (with the option cv.TM_CCOEFF_NORMED). An optimized algorithm for NMS is available in Ref. [35]. And intensity thresholding can be performed with the function *threshold_multiotsu* included in the Scikit-Image library.[9]

Ground Truth PSDs: The ground truth (GT) histograms of each of the five samples examined in this work were measured by manually annotating the TEM images. A drawing program was used to label the pixels of the images into one among two (particle-background) or three (particle-core-shell) classes. The labeled images were calibrated in nanometers (nm) and the diameters of the NPs were measured and saved as .txt files. The histograms shown in the figures were calculated using 30 bins and normalizing the distributions to the maximum counts value.

Statistical Definitions: The Area-equivalent diameter is defined like

$$D_i^{AE}=\sqrt{\frac{4A_i}{\pi}} \quad (2)$$

where the size of the particle is approximated to the diameter of a circle, D_i^{AE}, that has an area, A_i, equivalent to the area reported for the particle. The arithmetic mean diameter is defined like

$$\overline{D}^{AE}=\frac{\sum_{i=1}^{N}D_i^{AE}}{N} \quad (3)$$

and the standard deviation is defined like

$$std=\sqrt{\frac{\sum_{i=1}^{N}(D_i^{AE}-\overline{D}^{AE})^2}{N-1}} \quad (4)$$

The two-sample Kolgomorov–Smirnov (KS) test was applied to evaluate quantitatively if the normalized histograms measured automatically and the ground truth histograms came from the same distribution.[36] The KS test was carried out using the MATLAB 2021a function *kstest2* using a significance level of 0.05. The significance level is the probability of rejecting the null hypothesis when it is true, and indicates a 5% risk of concluding that a difference exists between histograms when there is no actual difference.

Supporting Information

Supporting Information is available from the Wiley Online Library or from the author.

Acknowledgements

The authors want to acknowledge funding from MCIU/AEI/ERDF-EU through projects PGC2018-101538-A-I00. Financial support from the program Plan Propio-UCA Ref 18INPPPR05 and from the grant Proyectos de I+D+i DE entidades públicas – Convocatoria 2020 P20_01206 (VERSO) are also acknowledged.

Conflict of Interest

The authors declare no conflict of interest.

Data Availability Statement

The data that support the findings of this study are available in the supplementary material of this article.

Keywords

electron microscopy, nanometrology, nanoparticles, transmission electron microscopy, template matching

Received: October 10, 2022
Revised: November 14, 2022
Published online: January 26, 2023

[1] W. J. Stark, P. R. Stoessel, W. Wohlleben, A. Hafner, *Chem. Soc. Rev.* **2015**, *44*, 5793.
[2] L. C. Gontard, R. Dunin-Borkowski, D. Ozkaya, T. Hyde, P. Midgley, P. Ash, in *Journal of Physics: Conference Series*, Vol. *26*, IOP Publishing, Bristol, England **2006**, p. 089.
[3] L. C. Gontard, R. E. Dunin-Borkowski, M. H. Gass, A. L. Bleloch, D. Ozkaya, *Med. Electron Microsc.* **2009**, *58*, 167.
[4] C. R. Laramy, K. A. Brown, M. N. O'Brien, C. A. Mirkin, *ACS Nano* **2015**, *9*, 12488.
[5] B. Lee, S. Yoon, J. W. Lee, Y. Kim, J. Chang, J. Yun, J. C. Ro, J.-S. Lee, J. H. Lee, *ACS Nano* **2020**, *14*, 17125.
[6] F. Wang, H. Gong, G. Liu, M. Li, C. Yan, T. Xia, X. Li, J. Zeng, *J. Struct. Biol.* **2016**, *195*, 325.
[7] X. Wang, J. Li, H. D. Ha, J. C. Dahl, J. C. Ondry, I. Moreno-Hernandez, T. Head-Gordon, A. P. Alivisatos, *Jacs Au* **2021**, *1*, 316.
[8] N. Otsu, *IEEE Trans. Syst. Man Cybern. A Syst.* **1979**, *9*, 62.
[9] P.-S. Liao, T.-S. Chen, P.-C. Chung, *J. Inf. Sci. Eng.* **2001**, *17*, 713.
[10] R. Fisker, J. M. Carstensen, M. F. Hansen, F. Bødker, S. Mørup, *J. Nanopart. Res.* **2000**, *2*, 267.
[11] L. Cervera Gontard, D. Ozkaya, R. E. Dunin-Borkowski, *Ultramicroscopy* **2011**, *111*, 101.
[12] L. C. Gontard, M. Á. Cauqui, M. P. Yeste, D. Ozkaya, J. J. Calvino, *ChemCatChem* **2019**, *11*, 3171.
[13] S. Mondini, A. Ferretti, A. Puglisi, A. Ponti, *Nanoscale* **2012**, *4*, 5356.
[14] M. van Sebille, L. J. van der Maaten, L. Xie, K. Jarolimek, R. Santbergen, R. A. van Swaaij, K. Leifer, M. Zeman, *Nanoscale* **2015**, *7*, 20593.
[15] M. Mirzaei, H. K. Rafsanjani, *Micron* **2017**, *96*, 86.
[16] Y. Meng, Z. Zhang, H. Yin, T. Ma, *Micron* **2018**, *106*, 34.
[17] S. Zafari, T. Eerola, P. Ferreira, H. Kälviäinen, A. Bovik, in *International Conference on Computer Analysis of Images and Patterns*, Springer, Salerno, Italy **2019**, pp. 113–125.
[18] H. Wen, X. Xu, S. Cheong, S.-C. Lo, J.-H. Chen, S. L. Chang, C. Dwyer, *Nanoscale Adv.* **2021**, *3*, 6956.
[19] A. V. Nartova, M. Y. Mashukov, R. R. Astakhov, V. Y. Kudinov, A. V. Matveev, A. G. Okunev, *Catalysts* **2022**, *12*, 135.
[20] D. M. Rubin, *J. Sediment. Res.* **2004**, *74*, 160.
[21] Z. Huang, P. A. Penczek, *J. Struct. Biol.* **2004**, *145*, 29.
[22] V. Abrishami, A. Zaldívar-Peraza, J. M. de la Rosa-Trevín, J. Vargas, J. Otón, R. Marabini, Y. Shkolnisky, J. M. Carazo, C. O. S. Sorzano, *Bioinformatics* **2013**, *29*, 2460.
[23] S. Mitchell, R. Qin, N. Zheng, J. Pérez-Ramírez, *Nat. Nanotechnol.* **2021**, *16*, 129.
[24] T. Malisiewicz, A. Gupta, A. A. Efros, presented at *International conference on computer vision*, Barcelona, Spain, November **2011**.
[25] L. S. Thomas, J. Gehrig, *BMC Bioinf.* **2020**, *21*, 1.
[26] S. B. Rice, C. Chan, S. C. Brown, P. Eschbach, L. Han, D. S. Ensor, A. B. Stefaniak, J. Bonevich, A. E. Vladár, A. R. H. Walker, J. Zheng, C. Starnes, A. Stromberg, J. Ye, E. A. Grulke, *Metrologia* **2013**, *50*, 663.
[27] M. Ulrich, C. Steger, *Int. Arch. Photogramm. Remote Sens. Spat. Inf. Sci.* **2002**, *34*, 368.
[28] L. C. Gontard, J. Pizarro, Á. Ruiz-Zafra, J. Hernández-Saz, *Mater. Charact.* **2020**, *164*, 110312.
[29] L. Mill, D. Wolff, N. Gerrits, P. Philipp, L. Kling, F. Vollnhals, A. Ignatenko, C. Jaremenko, Y. Huang, O. De Castro, J.-N. Audinot, I. Nelissen, T. Wirtz, A. Maier, S. Christiansen, *Small Methods* **2021**, *5*, 2100223.
[30] J. P. Horwath, D. N. Zakharov, R. Mégret, E. A. Stach, *npj Comput. Mater.* **2020**, *6*, 1.
[31] L. C. Gontard, B. R. Knappett, A. E. Wheatley, S. L.-Y. Chang, A. Fernandez, *Carbon* **2014**, *76*, 464.
[32] G. Walther, L. Cervera-Gontard, U. Quaade, S. Horch, *Gold Bull.* **2009**, *42*, 13.
[33] L. C. Gontard, R. E. Dunin-Borkowski, *Micron* **2015**, *70*, 41.
[34] T. Malisiewicz, blazing fast nms.m (from exemplar-svm library), **2011**, https://www.computervisionblog.com/2011/08/blazing-fast-nmsm-from-exemplar-svm.html.
[35] A. Rosebrock, (faster) non-maximum suppression in python, **2015**, https://pyimagesearch.com/2015/02/16/faster-non-maximum-suppression-python/.
[36] F. J. Massey Jr., *J. Am. Stat. Assoc.* **1951**, *46*, 68.

